Free fluid vesicles are not exactly spherical

Gunnar T. Linke,* Reinhard Lipowsky, and Thomas Gruhn
Max-Planck-Institut für Kolloid- und Grenzflächenforschüng, Am Mühlenberg 1, 14476 Golm, Germany
(Received 21 December 2004; published 5 May 2005)

At finite temperature, vesicles perform small fluctuations around an average shape. In the limit of low temperature or high bending rigidity, the fluctuations vanish and the vesicle approaches the energetically favored configuration. In the absence of a volume constraint the configuration of lowest energy is a perfect sphere. It is often assumed that the spherical shape is also the most probable shape for finite temperatures. Consequently, a force would have to be applied to make the average shape of the vesicle anisotropic. In this article it is shown that these assumptions are incorrect. At finite temperature, the most probable shapes of a vesicle without volume constraint are prolate or oblate, where the probability for prolate shapes is slightly larger. For larger deviations from the sphere the vesicle behaves as expected. The behavior at small deformations that is found for vesicles without volume constraint as well as in the presence of a finite osmotic pressure is basically an entropic effect. It already occurs in a three-dimensional crossed dumbbells model system. In two dimensions the same model favors the isotropic state.

DOI: 10.1103/PhysRevE.71.051602 PACS number(s): 68.15.+e, 87.16.Dg, 87.16.Ac

I. INTRODUCTION

Vesicles are closed membranes that can perform shape fluctuations on roughly all length scales between the membrane thickness and the vesicle diameter. In the simplest case the bending energy of the vesicle can be written as [1,2]

$$E_{\mathrm{el}} = \frac{\kappa}{2} \oint (2M)^2 dA \tag{1}$$

where κ denotes the bending rigidity and M is the mean curvature. The shapes of free and adhering vesicles that minimize the free energy (1) have been studied systematically [3,4]. These minimal free energy shapes do not include the effects of thermally excited fluctuations which are present for any finite temperature $T>0$. The influence of temperature on adhered vesicles has recently been studied [5].

With standard optical microscopy, only structures that are larger than about 0.5 μm can be resolved. The shape analysis of vesicles is therefore typically applied to the visible, so-called projected membrane surface [6,7], which is an averaged, coarse-grained image of the true, microscopic vesicle shapes. While the total microscopic surface area is approximately fixed, one finds a finite area fluctuation for the projected surface. Further, the bending rigidity κ in Eq. (1) depends on the length scale on which the integral is evaluated. Fluctuations of a planar membrane can be expanded in a Fourier series. In this case the average area fluctuation [6] and the renormalized bending rigidity [8,9] can be calculated exactly.

Several methods have been developed to measure the bending rigidity of a vesicle. For a vesicle sucked into a micropipet the bending rigidity can be determined from a comparison with minimized energy shapes [10–12] or by considering the fluctuations of the vesicle surface outside the pipet [13,14]. For free vesicles κ can be measured by pulling tethers out of the vesicle surface [15–17] or by doing Fourier analysis of shape fluctuations [18–21]. For adhered vesicles a method for obtaining κ by measuring the temperature dependence of the adhesion area has recently been proposed [5]. In this article we restrict ourselves to vesicles of genus zero, which have the same topology as a sphere.

For vesicles with a fixed reduced volume, smaller than that of a sphere, vesicle shapes are preferentially prolate or oblate [22]. The vesicle can change from prolate to oblate via intermediate biaxial configurations. In addition, it was also shown that, in the spherical limit, nontrivial shape transformations occur at constant elastic energy [23]. On the other hand, previous studies on vesicles with free volume and large enough bending rigidity have tacitly assumed that the corresponding vesicle shapes oscillate around the spherical shape, which has the lowest potential energy. Therefore, the shape of such vesicles is typically expanded in spherical harmonics [4,24]. In contrast, we show in this article that such vesicles are not preferentially spherical. Instead, prolate and oblate shapes are preferred. This anisotropy is of entropic origin. A similar effect of entropy-driven spontaneous anisotropy has also been found for closed random walk polymers without bending stiffness [25].

In Sec. II we define a measure for the deviation of a vesicle's shape from a sphere. Some simulation details for performing Monte Carlo simulations in order to measure such deformations are given in Sec. III; the results are presented in Sec. IV. Subsequently, a minimal model for this system is introduced in Sec. V and compared with a similar model in two dimensions (Sec. VI).

II. MEASURING THE DEVIATIONS FROM A SPHERE

In order to quantify the deviation of the vesicle from a spherical shape, a suitable order parameter is needed. Anisotropy of nonpolar media is typically measured by a second-rank tensor. A good choice turns out to be the inertia tensor of the compartment of the vesicle,

*Electronic address: linke@mpikg-golm.mpg.de

$$\mathcal{I}_{ij} \equiv -\int_V d^3r\left(\hat{r}_i\hat{r}_j - \delta_{ij}\sum_k \hat{r}_k\hat{r}_k\right) \quad \text{with } \hat{r}_i = \frac{1}{V}\int_V d^3r'(r_i - r_i'), \tag{2}$$

which is almost constant with respect to small-wavelength fluctuations of the vesicle surface.

If the vesicle is approximately a sphere, the lowest deformation mode transforms this sphere into an ellipsoid. Let e_i, $i=1,2,3$, be the eigenvalues of the tensor of inertia with respect to the center of mass, which we order in such a way that e_1 and e_2 have the smallest difference, i.e., $|e_1-e_2| \leqslant |e_i-e_j|$ $(i \neq j)$. We then introduce the deformation parameter

$$d \equiv 1 - 2\frac{e_3}{e_1+e_2} \tag{3}$$

as a measure for the anisotropy of the vesicle shape. In the case of an ellipsoid of revolution the eigenvector of e_3 is parallel with the symmetry axis; the parameter d vanishes for a sphere and converges to +1 for the maximum prolate and to −1 for the maximum oblate configuration. Note that $0 \leqslant e_3 \leqslant e_1+e_2$ and thus $-1 \leqslant d \leqslant 1$ by definition of the inertia tensor.

III. MONTE CARLO SIMULATIONS

With the help of Monte Carlo simulations, we estimate the probability distribution $p(d)$ of the anisotropy of a vesicle at finite temperature T.[1] For a given value of d we define the restricted partition sum

$$Z(d) \equiv \int d\Gamma \exp\left(-\frac{E(\Gamma)}{T}\right)\delta(d'(\Gamma) - d), \tag{4}$$

where the integration takes place over the whole configuration space. With

$$Z_{\text{total}} = \int_{-1}^{1} d\lambda\, Z(\lambda), \tag{5}$$

and the restricted free energy [26]

$$F(d) = -T \ln Z(d), \tag{6}$$

the probability density $p(d)$ reads

$$p(d) = \frac{\exp[-F(d)/T]}{Z_{\text{total}}}. \tag{7}$$

Previous algorithms were based on overlapping intervals [27,28]. This algorithm turns out to be impractical and computationally too demanding for the systems concidered here since the Markov chain of Monte Carlo steps diffuses only slowly within the configuration space. Therefore, we developed a modified algorithm which is based on nonoverlapping intervals. For each value d_m, the size $2\Delta d$ of the interval is chosen in such a way that one can obtain a reliable estimate for $\partial F/\partial d$ at $d_m = d$. The free energy $F(d)$ is then obtained by integration of $\partial F/\partial d$, where it is implicitly assumed that $F(d)$ is smooth between d_m and d_{m+1}.

In our Monte Carlo simulations, the fluid vesicle is represented by a closed, dynamically triangulated surface with 500 vertices and edge lengths according to the tethered-beads model [29–32]. Three types of Monte Carlo moves are applied: (i) independent moves of single vertices make 39% of the attempted moves, (ii) bond flips [32] in which an edge between two triangles is relocated to connect the formerly unconnected vertices of the two triangles make 59% of all moves, and (iii) changes of the deformation parameter d within the interval $d_m - \Delta d \leqslant d \leqslant d_m + \Delta d$ are the remaining 2%.

The bond flips ensure membrane fluidity. Moves of type (iii) distinctly improve the simulation performance. In moves of type (iii), the vesicle can be stretched or compressed with respect to the center of mass and a principal axis of inertia, which is chosen randomly with equal probability. Under this procedure the eigenvectors remain unchanged. Thus, only the detailed balance for stretching and compression parallel to the chosen principal axis of inertia must be ensured. Let m_i and m_i' denote the maximum distance of the vesicle surface from the center in the direction of the chosen principal axis of inertia before and after a trial transformation, and let $p(m_i \to m_i')$ be the conditional probability density for accepting this deformation. With a probability $q(m_i'|m_i)$ for choosing a stretching factor m_i'/m_i (given m_i), detailed balance demands

$$\frac{p(m_i \to m_i')}{p(m_i' \to m_i)}\frac{q(m_i'|m_i)}{q(m_i|m_i')} = \frac{\exp[-E(e_i')/T]}{\exp[-E(e_i)/T]}. \tag{8}$$

With the probability density of the standard Metropolis algorithm [33]

$$p(m_i \to m_i') = \min\left\{1, \exp\left(-\frac{E(m_i') - E(m_i)}{T}\right)\right\} \tag{9}$$

detailed balance is achieved if $q(m_i'|m_i) = q(m_i|m_i')$. The simplest choice for q is

$$q(m_i'|m_i) = \begin{cases} \dfrac{1}{2\delta} & \text{if } m_i - \delta \leqslant m_i' \leqslant m_i + \delta, \\ 0 & \text{else,} \end{cases} \tag{10}$$

with a maximal deviation $\delta > 0$. Due to the elastic energy of the vesicle, configurations with negative m' do not occur. We used $\delta = 0.03$ which gives a sufficiently large acceptance rate when applied to the tethered-beads model.

In general, the total energy E of a vesicle is given by $E = E_{\text{el}} + E_{\text{osm}}$ where E_{el} is the bending energy as given in Eq. (1) and E_{osm} is the osmotic pressure contribution. The spontaneous curvature is taken to be zero.

For the discretized vesicle surface, an adequate discretization of the local mean curvature is required [34,35]. We have applied a triangle-based calculation scheme as used by Kumar *et al.* [36]

[1] For simplicity, we set the Boltzmann constant to one. All simulations were done at $T=1$.

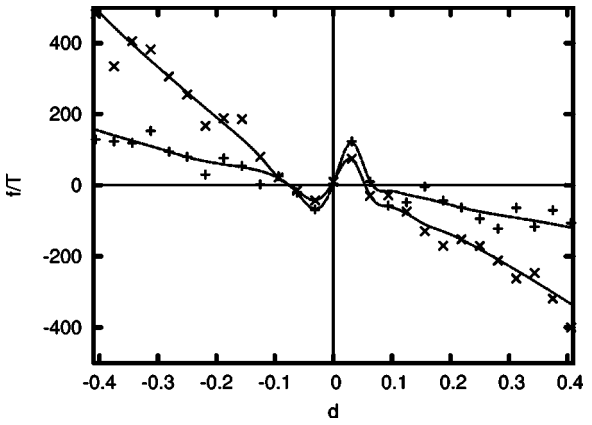

FIG. 1. Generalized force $f(d)=-\partial F/\partial d$ in units of the thermal energy T for $\kappa=10T$ (+) and $\kappa=30T$ (×). The lines are guides to the eye.

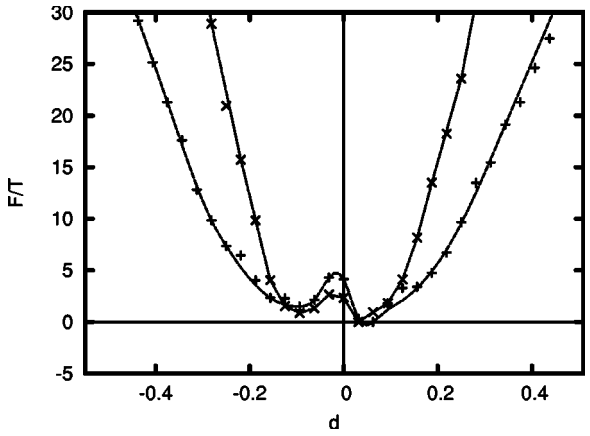

FIG. 2. Free energy $F(d)$ in units of the thermal energy T for $\kappa=10T$ (+) and $\kappa=30T$ (×). The lines are guides to the eye.

The fluid inside and outside the vesicle may contain large molecules or particles which cannot diffuse through the vesicle membrane. In this case the vesicle is affected by an osmotic pressure that leads to the osmotic free energy [4,37]

$$E_{\mathrm{osm}} = c_{\mathrm{ex}} T\left(V - V_{\mathrm{osm}} \ln \frac{V}{V_0}\right), \tag{11}$$

where c_{ex} is the concentration of such molecules outside the vesicle, V is the vesicle volume, V_0 is some reference volume which depends on the number of degrees of freedom of the osmotically active particles, and V_{osm} is the osmotically preferred volume, defined as $V_{\mathrm{osm}}=N/c_{\mathrm{ex}}$. Here, N is the number of osmotically active particles inside the vesicle. Typical experimental osmolarities are so large that the vesicle volume is almost constant.

IV. SIMULATION RESULTS

The global elastic properties of vesicles depend sensitively on the bending rigidity κ and the osmotic pressure that acts on the vesicle. In the following the influence of the two parameters on the average vesicle deformation d is studied separately. All energies are given in units of T while lengths are in units of $\sqrt{A/4\pi}$ where A is the total area of the membrane.

A. Zero osmotic pressure

For zero temperature, the vesicle surface that minimizes the elastic energy is a sphere. Since this minimal elastic energy is a smooth function of the deformation d, it can be expanded around $d=0$ for a spherical shape giving a generalized force $f_{\mathrm{el}}(d)=-\partial E_{\mathrm{el}}/\partial d \sim d$ for small values of d. Usually, it is assumed that this relation holds also for finite temperature.

The generalized force has been obtained in a sequence of Monte Carlo simulations. Results are shown in Fig. 1. One finds that in the range of $0.2 \lesssim |d| \lesssim 0.5$ the curves of $f_{\mathrm{el}}(d)$ are approximately proportional to d, but for $|d|<0.2$ the forces show a surprising behavior. At $d \simeq \pm 0.1$ the forces vanish with $\partial f/\partial d<0$. Further, we have $f(d=0)=0$ with $\partial f/\partial d>0$ (Fig. 1). This means, we have local minima in the associated free energy at $d \approx \pm 0.1$ and a local maximum at $d=0$ (Fig. 2). Thus, fluid vesicles tend to be either prolate or oblate with deformation parameter $d \approx \pm 0.1$ rather than spherical. Integration of the force shows that the minimum at $d \simeq 0.1$ is slightly deeper than that at $d \simeq -0.1$ (Fig. 2), i.e., the vesicles are preferentially prolate. This effect does not depend on the number of vertices used in the triangulation as shown in Fig. 3.

One should note that a prolate shape can be transformed continuously into an oblate one via biaxial shapes in such a way that no intermediate shape corresponds to a sphere. During this process, the asphericity parameter d changes its sign discontinuously as the order of eigenvalues e_i changes. For example, if we have $e_1=4$, $e_2=5+\epsilon$, and $e_3=6$ and vary ϵ continuously around zero, then we observe a jump in d from $-\frac{1}{3}$ to $\frac{3}{11}$ at $\epsilon=0$. Thus, the maximum of $F(d)$ at $d=0$ is not a barrier that the vesicle must overcome in order to change from prolate to oblate.

B. Nonzero osmotic pressure

In the presence of osmotically active particles the vesicle is exposed to an osmotic pressure

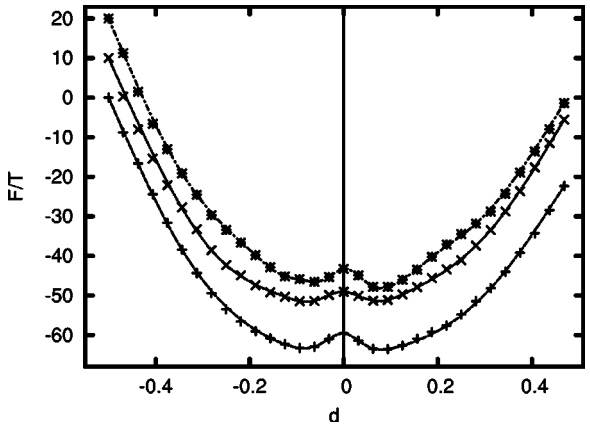

FIG. 3. Free energy $F(d)$ (with arbitrary offset) in units of the thermal energy T for different numbers of vertices $n=300$ (+), 400 (×), and 500 (*), $\kappa=15T$. The lines are guides to the eye.

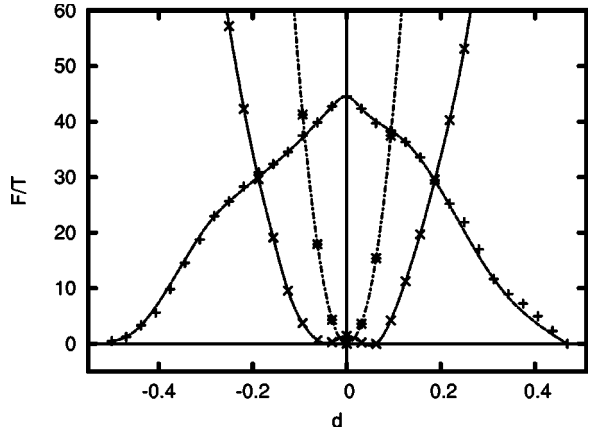

FIG. 4. Free energy $F(d)$ in units of the thermal energy T for $N=10\,000$ and $V_{\mathrm{osm}}/V_{\mathrm{max}}=0.8$ (+), $N=15\,000$ and $V_{\mathrm{osm}}/V_{\mathrm{max}}=1.2$ (×), $N=30\,000$ and $V_{\mathrm{osm}}/V_{\mathrm{max}}=2.4$ (*), $c_{\mathrm{ex}}=3000$, $\kappa=15T$. The lines are guides to the eye.

$$P_{\mathrm{osm}} = c_{\mathrm{ex}} T \left(\frac{V_{\mathrm{osm}}}{V} - 1 \right), \tag{12}$$

which would vanish at $V=V_{\mathrm{osm}}=N/c_{\mathrm{ex}}$. For a vesicle with a surface area $A=4\pi R_0^2$ the volume cannot be larger than $V=V_{\mathrm{max}}=(4\pi/3)R_0^3$, which corresponds to a spherical vesicle. For $V_{\mathrm{osm}}/V_{\mathrm{max}}<1$ the osmotic pressure favors a nonspherical vesicle shape. For $V_{\mathrm{osm}}>V_{\mathrm{max}}$ it favors shapes of low anisotropy. If N is increased while V_{osm} is kept constant, the average vesicle volume approaches V_{osm}.

In Fig. 4, the restricted free energy $F(d)$ is shown for $V_{\mathrm{osm}}/V_{\mathrm{max}}=0.8$, 1.2, and 2.4. For $V_{\mathrm{osm}}/V_{\mathrm{max}}=0.8$ minima are found at $d\simeq\pm0.5$ (see Fig. 5 for typical conformations) and for $V_{\mathrm{osm}}/V_{\mathrm{max}}=2.4$ there is one minimum at $d\simeq0$, as expected from the considerations above. At $V_{\mathrm{osm}}/V_{\mathrm{max}}=1.2$, however, minima are found at $d\simeq\pm0.05$. Apparently, in this case the entropy-induced asphericity is not compensated by the bending rigidity and the osmotic pressure, which both favor $d\simeq0$.

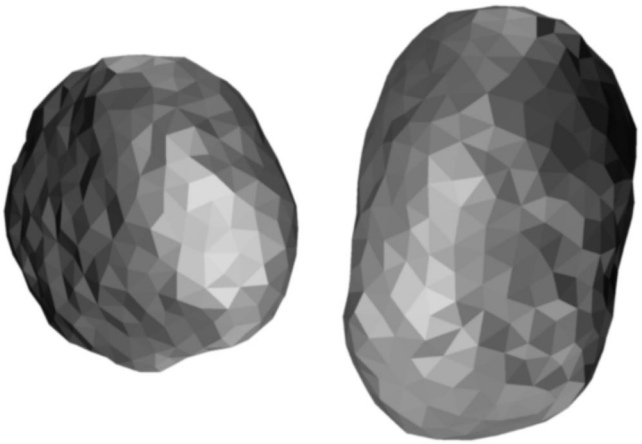

FIG. 5. Typical conformations for $d=-0.5$ (left) and 0.47 (right) with $N=10\,000$, $c_{\mathrm{ex}}=3000$, $\kappa=15T$.

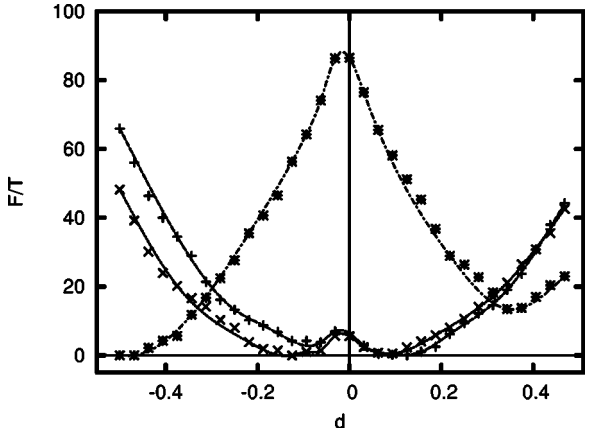

FIG. 6. Free energy $F(d)$ in units of the thermal energy T for $\kappa=15T$ and different homogeneous fields $g=5T$ (+), $50T$ (×), and $500T$ (*). The lines are guides to the eye.

In summary, we have found that if a vesicle is exactly spherical, it must be stabilized by a sufficiently strong osmotic pressure. Otherwise the stable shape of a vesicle at finite temperature is slightly prolate or oblate.

C. Gravity effects

In many vesicle experiments the influence of the gravitational force cannot be neglected. Thus, it is of great interest to study the influence of gravity on the asphericity of vesicle shapes.

We have simulated a fluid vesicle on a hard wall (at $z=0$) without the influence of osmotic effects but in a homogeneous field with an associated energy contribution $E_{\mathrm{gravi}}=gb_z$ where w is the potential strength and b_z is the z coordinate of the center of mass of the vesicle shell. The vesicle shell is assumed to have constant mass and spatial mass density. For the small value $g=5T$ the total minimum of $F(d)$ is located at $d\simeq0.1$, corresponding to a prolate vesicle (Fig. 6). This is in accordance with calculations by Kraus *et al.* for reduced volumes of $v\simeq0.8$ in the stationary case [38]. For a strong field $g=500T$ the free energy $F(d)$ has its minimum at $d\simeq-0.5$ so that the vesicles are preferentially oblate (Fig. 6).

V. CROSSED DUMBBELLS MODEL

The spontaneous asphericity of the vesicles appears to be an entropic effect. This is tested by considering a rather simple model system where all degrees of freedom of the vesicle membrane are removed apart from the lowest fluctuation mode in three dimensions. Let us consider six mass points with equal masses located on the three (pairwise perpendicular) coordinate axes. The distances L_i of the mass points from the origin are equal for the two points on each axis (Fig. 7), and the six mass points form three crossed dumbbells which have their centers of mass always at the origin. The values of the distances L_i are independently distributed according to the same probability density function q with $q(x)=0$ for $x\leqslant0$. This function q is chosen in such a way that it is centered around $x=1$ with a half-width λ.

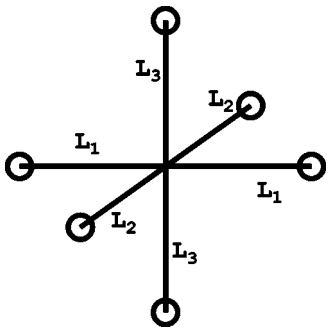

FIG. 7. crossed dumbbells model in three dimensions. Description in the text.

With the definition $a_i \equiv L_i^2$, the inertia tensor $\mathcal{I}$ of Eq. (2) is given by

$$\mathcal{I} = \begin{pmatrix} a_2 + a_3 & 0 & 0 \\ 0 & a_1 + a_3 & 0 \\ 0 & 0 & a_1 + a_2 \end{pmatrix}. \tag{13}$$

Obviously, we have $|e_i - e_j| = |a_i - a_j|$. For symmetry reasons we restrict ourselves to the case where $0 \leqslant a_1 \leqslant a_2 \leqslant a_3$. The remaining cases are found by permutations, which gives an extra factor of 6 in the partition function. As shown in the Appendix the probability density $p(d)$ is approximately given by

$$p(d) \approx p_0 \frac{|d|(3-2d)}{(3-d)^2(1-d)^2} \quad \text{for } d \ll \lambda \tag{14}$$

with a normalization constant p_0 which depends on q. Focusing on almost isotropic configurations with very small d, we make a linear approximation of $p(d)$ around $d=0$,

$$p(d) \approx \frac{p_0}{4}|d|. \tag{15}$$

Obviously the probability density for $d=0$ is zero while it increases with the same slope for $d>0$ and $d<0$. From Eq. (14) it follows that for larger $|d|$ the prolate branch of $p(d)$ with $d>0$ grows faster than the oblate one. This is shown in Fig. 8.

The probability density $p(d)$ is related to the restricted free energy by $F(d) = -T \ln p(d) + F_0$ with a deformation-independent offset F_0 and to the associated generalized force by $f(d) = Tp'(d)/p(d)$. Thus, for the minimized model the amplitude of the generalized force $f(d) \approx T/d$ goes to infinity as d goes to zero.

The crossed dumbbells model has three degrees of freedom which are completely independent and do not experience any crumpling. Nevertheless, the system exhibits some spontaneous anisotropy which therefore appears to be a purely entropic effect. In fact, for the crossed dumbbell system, the avoidance of the isotropic state is extremely strong. For vesicles, this effect is weakened by the mutual interactions of the deformation modes. Furthermore, an additional constraint arising, e.g., from a sufficiently strong osmotic pressure can destroy the spontaneous anisotropy.

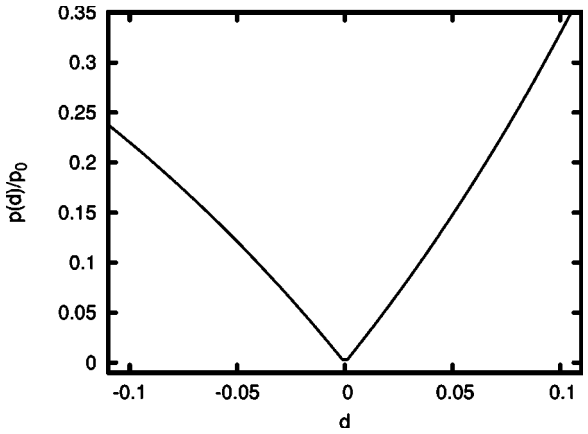

FIG. 8. Probability density function p for the deformation parameter d as in Eq. (14).

VI. DIFFERENT RESULTS IN TWO AND THREE DIMENSIONS

In the previous section spontaneous anisotropy is found in a simple three-dimensional model. The question is whether the same effect can also be obtained in two dimensions.

Let us consider a two-dimensional analog (Fig. 9) to the minimized model in the previous section.

In two dimensions, the ratio of the square roots of the two eigenvalues a^2 and b^2 of the inertia tensor characterizes the deformation state. In order to have a deformation measure d which does not depend on the order of the eigenvalues we define

$$d_2 \equiv \max\left\{\frac{a}{b}, \frac{b}{a}\right\} \geqslant 1. \tag{16}$$

Let us assume that q is the joint probability density function of a and b. By definition, it is symmetric in its arguments. Let P denote the distribution function of d_2 and p its density. Doing the same procedure as in the last section, we find

$$P(d_2) = p_0 \int_{b=0}^{\infty} db \left(\int_{a=b}^{bd_2} da\, q(a,b) \right), \tag{17}$$

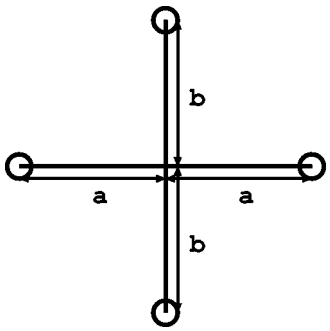

FIG. 9. crossed dumbbells model in two dimensions. Description in the text.

$$p(d_2) = P'(d_2) = p_0 \int_{b=0}^{\infty} db\, bq(bd_2, b) \tag{18}$$

with the normalization constant

$$p_0 = \frac{2}{\int_0^\infty da \int_0^\infty db\, q(a,b)}. \tag{19}$$

If we assume q to be a Gaussian centered around $a=b=\mu$ with half-width λ in the $a=b$ direction, we get the intuitive result

$$p(d_2) \approx p_0(2 - d_2) \tag{20}$$

with a finite probability for symmetric configurations ($d_2 \gtrsim 1$) in contrast to the counterintuitive result for three dimensions.

Assuming q to be a Gaussian is not the only choice, but it is easy to see that $p(d_2)$ is positive and continuous at $d_2 \geqslant 1$ for any reasonable choice of q.

VII. DISCUSSION

The conformation of fluid three-dimensional vesicles has been studied. Using Monte Carlo simulations, we have shown that for these vesicles anisotropic configurations are preferred to spherical shapes while oblate and prolate configurations are almost equiprobable for preset reduced volumes close to 1. This effect seems to be an entropic one since it is found in a minimized model where all but entropic effects are removed. It depends on the dimension as it does not exist in two dimensions.

APPENDIX: CALCULATIONS FOR THE CROSSED DUMBBELLS MODEL IN THREE DIMENSIONS

In Sec. V the three-dimensional crossed dumbbells model was introduced. We derive the distribution function $P(d_0)$, which gives the probability that the anisotropy parameter d of the minimized model introduced in Sec. V is smaller than d_0. For symmetry reasons we restrict ourselves to the case $0 < a_1 \leqslant a_2 \leqslant a_3$.

Let us first assume that $a_3 - a_2 \geqslant a_2 - a_1$ which means

$$a_3 \geqslant 2a_2 - a_1 \geqslant a_2. \tag{A1}$$

Furthermore, the integration range is restricted by

$$d = \frac{2a_3 - a_1 - a_2}{2a_3 + a_1 + a_2} \leqslant d_0,$$

which gives

$$a_3 \leqslant \frac{1 + d_0}{2(1 - d_0)}(a_1 + a_2). \tag{A2}$$

Since the inequalities (A1) and (A2) have to be satisfied simultaneously, we find

$$a_2 \geqslant a_1 \geqslant \frac{3 - 5d_0}{3 - d_0} a_2. \tag{A3}$$

This is only possible if $d_0 \leqslant 0$.

Let us now assume the opposite case $a_3 - a_2 \leqslant a_2 - a_1$ and thus

$$0 < a_1 \leqslant 2a_2 - a_3 \leqslant a_2 \tag{A4}$$

and

$$a_3 \leqslant 2a_2. \tag{A5}$$

In addition we have

$$d = \frac{2a_1 - a_2 - a_3}{2a_1 + a_2 + a_3} \leqslant d_0$$

and equivalently

$$a_1 \leqslant \frac{1 + d_0}{2(1 - d_0)}(a_2 + a_3). \tag{A6}$$

Depending on the value of d, either (A4) or (A5) defines the upper boundary for a_1: Since $|d| \leqslant 1$ it follows from (A6) that $a_3 \leqslant [(3-5d_0)/(3-d_0)]a_2$ which contradicts $a_3 \geqslant a_2$ for positive d_0. The integration range for arbitrary positive a_2 is thus given by

$$a_2 \leqslant a_3 \leqslant 2a_2 \quad \text{and} \quad 0 \leqslant a_1 \leqslant 2a_2 - a_3 \tag{A7}$$

for $0 \leqslant d_0 \leqslant 1$. For $-1 \leqslant d_0 \leqslant 0$ we get

$$\left| \begin{array}{ll} a_2 \leqslant a_3 \leqslant \dfrac{3 - 5d_0}{3 - d_0} a_2 & \text{and} \quad 0 \leqslant a_1 \leqslant \dfrac{1 + d_0}{2(1 - d_0)}(a_2 + a_3) \\ & \text{or} \\ \dfrac{3 - 5d_0}{3 - d_0} a_2 \leqslant a_3 \leqslant 2a_2 & \text{and} \quad 0 \leqslant a_1 \leqslant 2a_2 - a_3 \end{array} \right|. \tag{A8}$$

Having determined the integration ranges for all a_1, a_2, and a_3 with $0 < a_1 \leqslant a_2 \leqslant a_3$, we are now able to give an expression for the distribution function P of d. Let us first assume $d \geqslant 0$. Referring to the above determined integration ranges (A3) and (A7), we find

$$P(d) = \tilde{p}_0 \int_{a_2=0}^{\infty} da_2 q(a_2) \left\{ \int_{a_1=[(3-5d)/(3-d)]a_2}^{a_2} da_1 q(a_1) \times \int_{a_3=2a_2-a_1}^{[(1+d)/(2(1-d))](a_1+a_2)} da_3 q(a_3) + \int_{a_3=a_2}^{2a_2} da_3 q(a_3) \int_{a_1=0}^{2a_2-a_3} da_1 q(a_1) \right\} \tag{A9}$$

with the normalization constant

$$\tilde{p}_0 = 6 \left(\int_0^{\infty} da\, q(a) \right)^{-3}. \tag{A10}$$

If we assume that d is small compared to the half-width λ of q, we find for its derivative, i.e., the probability density of d

$$p(d) = P'(d) \approx \tilde{p}_0 \lambda q^3(1) \frac{8d(3-2d)}{(3-d)^2(1-d)^2}. \tag{A11}$$

In the second case, we have $d<0$ and find according to (A8)

$$P(d) = \tilde{p}_0 \int_{a_2=0}^{\infty} da_2 q(a_2) \left\{ \int_{a_3=a_2}^{[(3-5d)/(3-d)]a_2} da_3 q(a_3) \times \int_{a_1=0}^{[(1+d)/(2(1-d))](a_2+a_3)} da_1 q(a_1) + \int_{a_3=[(3-5d)/(3-d)]a_2}^{2a_2} da_3 q(a_3) \int_{a_1=0}^{2a_2-a_3} da_1 q(a_1) \right\} \tag{A12}$$

and with the same approximation as above,

$$p(d) = P'(d) \approx \tilde{p}_0 \lambda q^3(1) \frac{-8d(3-2d)}{(3-d)^2(1-d)^2}.$$

Obviously, the results for both cases can be written in a unified expression

$$p(d) = P'(d) \approx 8\tilde{p}_0 \lambda q^3(1) \frac{|d|(3-2d)}{(3-d)^2(1-d)^2} \tag{A13}$$

or with $p_0 = 8\tilde{p}_0 \lambda q^3(1)$

$$p(d) \approx p_0 \frac{|d|(3-2d)}{(3-d)^2(1-d)^2}. \tag{A14}$$

[1] P. B. Canham, J. Theor. Biol. **26**, 61 (1970).
[2] W. Helfrich, Z. Naturforsch. C **28**, 693 (1973).
[3] R. Lipowsky, Nature (London) **349**, 475 (1991).
[4] U. Seifert, Adv. Phys. **46**, 13 (1997).
[5] T. Gruhn and R. Lipowsky, Phys. Rev. E **71**, 011903 (2005).
[6] W. Helfrich and R.-M. Servuss, Nuovo Cimento Soc. Ital. Fis., D **3**, 137 (1984).
[7] J.-B. Fournier, A. Ajdari, and L. Peliti, Phys. Rev. Lett. **86**, 4970 (2001).
[8] L. Peliti and S. Leibler, Phys. Rev. Lett. **54**, 1690 (1985).
[9] F. David, in *Statistical Mechanics of Membranes and Surfaces*, edited by D. Nelson, T. Piran, and S. Weinberg (World Scientific, Singapore, 1989), Vol. 5, pp. 157–223.
[10] E. A. Evans, Biophys. J. **30**, 265 (1980).
[11] R. Kwok and E. Evans, Biophys. J. **35**, 637 (1981).
[12] E. Evans and D. Needham, J. Phys. Chem. **91**, 4219 (1987).
[13] E. Evans and W. Rawicz, Phys. Rev. Lett. **64**, 2094 (1990).
[14] E. Evans and W. Rawicz, Phys. Rev. Lett. **79**, 2379 (1997).
[15] L. Bo and R. E. Waugh, Biophys. J. **55**, 509 (1989).
[16] B. Božič, S. Svetina, B. Žekš, and R. E. Waugh, Biophys. J. **61**, 963 (1992).
[17] V. Heinrich, B. Božič, S. Svetina, and B. Žekš, Biophys. J. **76**, 2056 (1999).
[18] M. B. Schneider, J. T. Jenkins, and W. W. Webb, J. Phys. (France) **45**, 1457 (1984).
[19] H. Engelhardt, H. P. Duwe, and E. Sackmann, J. Phys. (France) Lett. **46**, L395 (1985).
[20] H. P. Duwe, J. Käs, and E. Sackmann, J. Phys. (France) **51**, 945 (1990).
[21] H.-G. Döbereiner, G. Gompper, C. K. Haluska, D. M. Kroll, P. G. Petrov, and K. A. Riske, Phys. Rev. Lett. **91**, 048301 (2003).
[22] H.-G. Döbereiner, and U. Seifert, Europhys. Lett. **36**, 325 (1996).
[23] M. A. Peterson, Phys. Rev. A **39**, 2643 (1989).
[24] S. T. Milner and S. A. Safran, Phys. Rev. A **36**, 4371 (1987).
[25] H. W. Diehl and E. Eisenriegler, J. Phys. A **22**, L87 (1989).
[26] D. Frenkel, in *Monte Carlo and Molecular Dynamics of Condensed Matter Systems*, edited by K. Binder and G. Ciccotti, Conference Proceedings Vol. 49 (SIF, Bologna, 1996), pp. 3–42.
[27] A. M. Ferrenberg and R. H. Swendsen, Phys. Rev. Lett. **61**, 2635 (1988).
[28] A. M. Ferrenberg and R. H. Swendsen, Phys. Rev. Lett. **63**, 1195 (1989).
[29] Y. Kantor, M. Kardar, and D. R. Nelson, Phys. Rev. Lett. **57**, 791 (1986).
[30] Y. Kantor and D. R. Nelson, Phys. Rev. Lett. **58**, 2774 (1987).
[31] Y. Kantor, M. Kardar, and D. R. Nelson, Phys. Rev. A **35**, 3056 (1987).
[32] D. M. Kroll and G. Gompper, Science **255**, 968 (1992).
[33] N. Metropolis, A. W. Rosenbluth, M. N. Rosenbluth, A. H. Teller, and E. Teller, J. Chem. Phys. **21**, 1087 (1953).
[34] G. Gompper and D. M. Kroll, J. Phys. I **6**, 1305 (1996).
[35] M. Kraus, Ph.D. thesis, Universität Potsdam, Potsdam, 1996.
[36] P. B. S. Kumar, G. Gompper, and R. Lipowsky, Phys. Rev. Lett. **86**, 3911 (2001).
[37] M. P. Allen and D. J. Tildesley, *Computer Simulation of Liquids*, 1st ed. (Oxford University Press, Oxford, 1989).
[38] M. Kraus, U. Seifert, and R. Lipowsky, Europhys. Lett. **32**, 431 (1995).